

Single-layer Skyrmions in a van der Waals antiferromagnet

A. Pozzi* and M. Mostovoy

Zernike Institute for Advanced Materials, University of Groningen,
Nijenborgh 4, 9747 AG Groningen, The Netherlands

(Dated: January 27, 2023)

Transition metal halides are quasi-two-dimensional van der Waals magnets that can potentially host antiferromagnetic (AFM) skyrmions induced by competing exchange interactions. We study theoretically magnetic states of Fe-doped NiBr₂ using spin interactions obtained by fitting experimental data. We find that AFM interlayer interactions suppress skyrmion lattices but allow for skyrmions with topological charges 1, 2 and 3 confined to a single magnetic layer. These single-layer skyrmions exist in three different magnetic phases and their dynamics changes drastically at the transition from a uniform to a non-collinear modulated state.

Since their first observation [1, 2], magnetic skyrmions are in the focus of many theoretical and experimental studies. Electrically driven dynamics and stability rooted in non-trivial topology make skyrmions promising information carriers in new magnetic memory devices [3–6]. Current research on skyrmions is focused on magnets with chiral crystal lattices and multilayer devices where inversion symmetry is broken at interfaces between magnetic and heavy-metal materials [7, 8]. The lack of inversion leads to anisotropic spin interactions favoring non-collinear magnetic textures [9].

Inversion symmetry breaking is not strictly necessary: the competing Heisenberg exchange interactions in Mott insulators [10–12] and long-ranged spin interactions mediated by itinerant electrons in magnetic conductors [13–16] can stabilize skyrmions and even more complex spin textures, such as hedgehog crystals [17]. Tiny (2-3 nm in diameter) skyrmions recently found in centrosymmetric intermetallics give rise to large Topological Hall and Nernst effects [18–21]. Isotropic interactions in achiral magnets result in additional low-energy skyrmion degrees of freedom, helicity and vorticity, which strongly modify interactions and dynamics of these topological defects [11, 22, 23]. There is also a lot of interest in skyrmions in natural and artificial AFM materials that may propagate with a higher speed and show no Skyrmion Hall effect [24–26].

Here, we explore the possibility to find skyrmions in layered transition metal halides, which are wide gap Mott insulators showing a variety of magnetic orders [27]. These van der Waals materials allow for exfoliation down to monolayers, which enables control of two-dimensional magnetism by doping, gating, magnetic and electric fields [28]. We focus on NiBr₂ that undergoes a transition into the collinear A-type AFM state at $T_N = 52$ K, which transforms into a multiferroic spiral state below 23 K with six energetically equivalent orientations of the in-plane wave vector [29–31]. The spin spiral results from the competition between the nearest-neighbor ferromagnetic (FM) Heisenberg exchange interactions on the $\sim 90^\circ$ metal-halogen-metal bonds and further-neighbor AFM interactions enhanced by strong metal-ligand covalency

and lattice geometry. The sign of magnetic anisotropy can be controlled in this material by doping [32].

Our study of a model of doped NiBr₂ with parameters obtained by fitting experimental data shows that the AFM interlayer interactions suppress skyrmion crystals at all magnetic fields and concentrations of dopands, but allow for topological defects with skyrmion topology, which are truly two-dimensional as their topological charge is only nonzero in a single magnetic layer. These single-layer skyrmions and bi-merons are stable in three different magnetic phases at experimentally accessible magnetic fields. We discuss dynamics of these defects induced by the spin-Hall torque.

The model. The spin Hamiltonian reads,

$$H = -J_1 \sum_{\langle i,j \rangle, \lambda} \mathbf{S}_i^\lambda \cdot \mathbf{S}_j^\lambda + J_2 \sum_{\langle\langle i,j \rangle\rangle, \lambda} \mathbf{S}_i^\lambda \cdot \mathbf{S}_j^\lambda + \sum_{i, \lambda} \left[J_\perp \mathbf{S}_i^\lambda \cdot \mathbf{S}_i^{\lambda+1} - \frac{K}{2} (S_i^\lambda)_z^2 - \mathbf{h} \cdot \mathbf{S}_i^\lambda \right], \quad (1)$$

where \mathbf{S}_i^λ denotes the unit spin vector at the site i of a triangular lattice in the layer λ . Indices in single and double brackets denote pairs of nearest-neighbor (NN) and next-nearest-neighbor (NNN) sites in the triangular lattice, respectively. The NN Heisenberg exchange interaction is ferromagnetic, whereas the NNN exchange that gives rise to frustration and the interlayer interaction are antiferromagnetic ($J_1, J_2, J_\perp > 0$); K is the single-ion anisotropy and \mathbf{h} is the magnetic field.

Equation (1) contains a few simplifications. First, NiBr₂ has a CdCl₂ crystal structure (space group $R\bar{3}m$) with ABC stacking of three triangular layers in the rhombohedral unit cell [27]. Second, the third-nearest-neighbor AFM exchange in NiBr₂ is stronger than the NNN one [33, 34]. Our model is justified by the long period of the spiral modulation (~ 18 in-plane lattice constants), which makes possible to ignore the relative shifts of neighboring layers. Spin models with 2 and 3 exchange interactions become equivalent in the continuum limit, the only difference being the orientation of the spiral wave vector. Earlier theoretical study of a single-layer frustrated triangular magnet with an easy-axis anisotropy

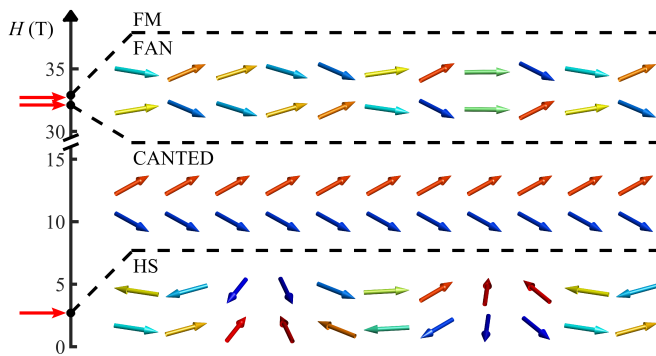


FIG. 1: Zero-temperature magnetic phase diagram of NiBr_2 in the magnetic field $H \perp c$. The black dots show the experimentally measured values of the three critical fields, $H_1 < H_2 < H_3$, corresponding to the transitions between the spiral, canted AFM, fan, and ferromagnetic spin states [36]. Red arrows indicate the critical fields obtained in our numerical simulations, for $J_1 = 59.5 \text{ K}$, $J_2 = 20.4 \text{ K}$ and $J_1 = 11.0 \text{ K}$. Spin configurations in two neighboring ab layers are schematically shown with arrows.

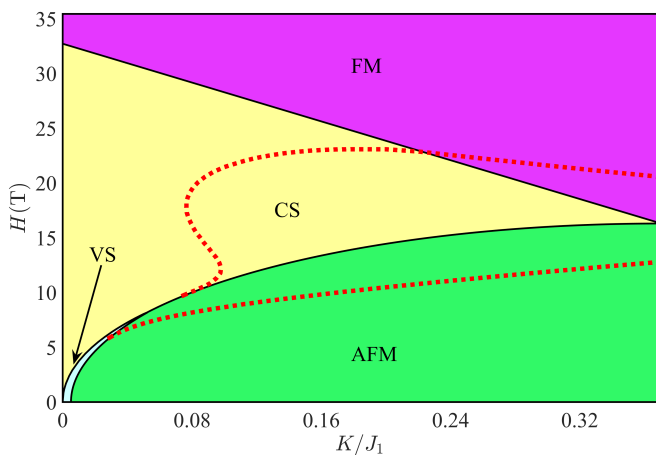


FIG. 2: Magnetic field vs anisotropy phase diagram of $\text{Fe}_x\text{Ni}_{1-x}\text{Br}_2$ for $H \parallel c$, which includes the A-type AFM, vertical spiral (VS), conical spiral (CS) and field-induced ferromagnetic (FM) states. The area encircled by red dotted line is the region of stability of defects with skyrmion charge ± 1 confined to a single spin layer.

($K > 0$) showed that the skyrmion crystal occupies a large part of the phase diagram [11]. NiBr_2 is an easy-plane antiferromagnet ($K < 0$) [33, 34], but its anisotropy changes sign upon substitution of magnetic ions: $\text{Fe}_x\text{Ni}_{1-x}\text{Br}_2$ becomes an easy-axis magnet for $x > 9.9\%$ [32]. AFM interlayer interactions in quasi-two-dimensional materials govern symmetry of skyrmion crystals and can suppress them [35]. The question arises whether the interlayer interactions in dihalides allow for skyrmions. To address this question, we determine exchange parameters of our model using experimental data on NiBr_2 . With

$J_2/J_1 = 0.343$ we fit the magnitude of the in-plane component of the spiral wave vector, $\mathbf{Q} = [0.027, 0.027, 3/2]$ [32] (see Supplementary Information). The interlayer coupling J_\perp is obtained from the fit of the phase diagram of NiBr_2 under an in-plane magnetic field [36], which shows three phase transitions: from the spiral to the canted AFM state at $H_1 = 2.7 \text{ T}$, from the AFM to the fan state at $H_2 = 31.5 \text{ T}$ and from the fan to saturated state at $H_3 = 32.9 \text{ T}$ measured at 1.3 K (see Fig. 1). The H_1/H_3 ratio is a measure of the ratio of the exchange energy difference between the uniform AFM and spiral states in zero field, ΔE_{ex} , and the interlayer exchange energy:

$$\frac{\Delta E_{\text{ex}}}{J_\perp} \simeq \left(\frac{H_1}{H_3} \right)^2 \approx 6.7 \cdot 10^{-3}. \quad (2)$$

Figure 1 shows the comparison between the critical fields obtained in our simulations for $J_\perp/J_1 = 0.184$ (red arrows) and experimentally measured values (black dots). We converted h into H measured in Tesla using $H = \frac{J_\perp}{2\mu_B} h$ with $J_1 = 59.5 \text{ K}$, $2\mu_B$ being the magnetic moment of Ni^{2+} ion. Since spins in all three magnetic phases are confined to the ab plane, the critical fields are independent of K .

Magnetic states and topological defects. Next we calculate the (H, K) phase diagram of the Fe-doped compound, $\text{Fe}_x\text{Ni}_{1-x}\text{Br}_2$, treating the anisotropy parameter K as a variable that depends on the concentration of Fe dopants x . Figure 2 shows the phase diagram for $K > 0$ (easy-axis anisotropy) and $H \parallel c$ including the vertical spiral (VS), A-type AFM, conical spiral (CS) and the field-polarized (FM) phases. The small energy difference between non-collinear and collinear spin orders [see Eq.(2)] confines the VS state to a narrow region between the A-type AFM state with alternating layers of spins parallel/antiparallel to the c axis and the CS phase, in which S^z is the same in all layers and the sign of the in-plane spiral component alternates from layer to layer. The skyrmion lattices, both the triangular array of skyrmion tubes and a three-dimensional HCP/FCC crystal of skyrmions [35], are suppressed for the realistic model parameters alongside with all multiply-periodic magnetic phases found a single triangular layer [10, 11].

Although the AFM interlayer coupling suppresses skyrmion crystals, it allows for isolated skyrmions with topological charge confined to a single layer. Remarkably, these single-layer skyrmions are stable in three different phases: the FM, AFM and CS states in the region encircled by red dotted line in Fig. 2. Figure 3a shows the skyrmion in the AFM state, which is only stable in layers with the magnetization opposite to the applied field. The magnetic moment in the skyrmion center is parallel to the field, in contrast to FM skyrmions (Fig. 3b). The small disturbance in the spin configuration of neighboring layers is topologically trivial (Fig. 3c) and its magnitude decays quickly with the distance from the skyrmion (see

Supplementary information). It has a stabilizing effect on skyrmions which are unstable in the surface layers.

Unexpectedly, a magnetic defect with skyrmion topology is also stable in the CS state (Fig. 4a). It has the appearance of a bi-meron – the bound vortex-antivortex pair [23], but its topological charge distribution has a single maximum and is not divided into two halves (see Fig. 4c). We also found single-layer skyrmions with topological charges $Q = \pm 2$ and ± 3 in the FM state (Figs. 4b,c) stabilized by AFM interlayer interactions.

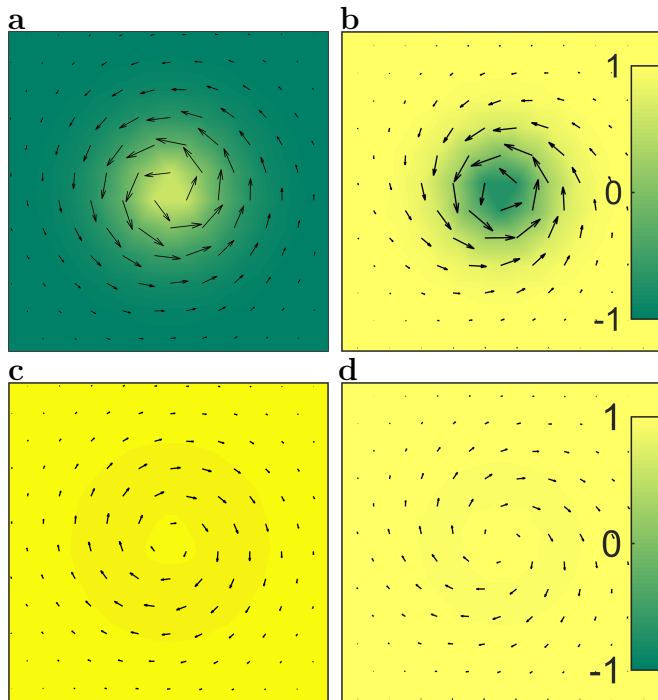


FIG. 3: Spin configurations in the layers containing the skyrmion in the (a) A-type AFM state and (b) FM state. (c) and (d) The corresponding spin configurations in neighboring layers. In-plane spin components are shown with arrows; the out-of-plane spin components are color coded.

Dynamics: Next we discuss dynamics of single-layer skyrmions induced by the spin-Hall torque [37, 38]

$$\mathbf{T}_{\text{SH}} \propto \mathbf{S} \times \mathbf{S} \times (\hat{\mathbf{c}} \times \mathbf{j}_c), \quad (3)$$

where \mathbf{j}_c is the charge current in a heavy metal layer generating a spin accumulation at the interface with the antiferromagnet, \mathbf{S} is a spin in the interface layer (layer 1) and the unit vector $\hat{\mathbf{c}}$ is normal to spin layers. Due to the instability of skyrmions at the interface, we study their dynamics in layer 2 (next to the interface layer) by numerical integration of Landau-Lifshitz-Gilbert equation with the torque (see Supplementary information).

The skyrmion in the uniform AFM and FM states shows the coupled helicity and center-of-mass dynamics [22] with the helicity angle growing linearly with time,

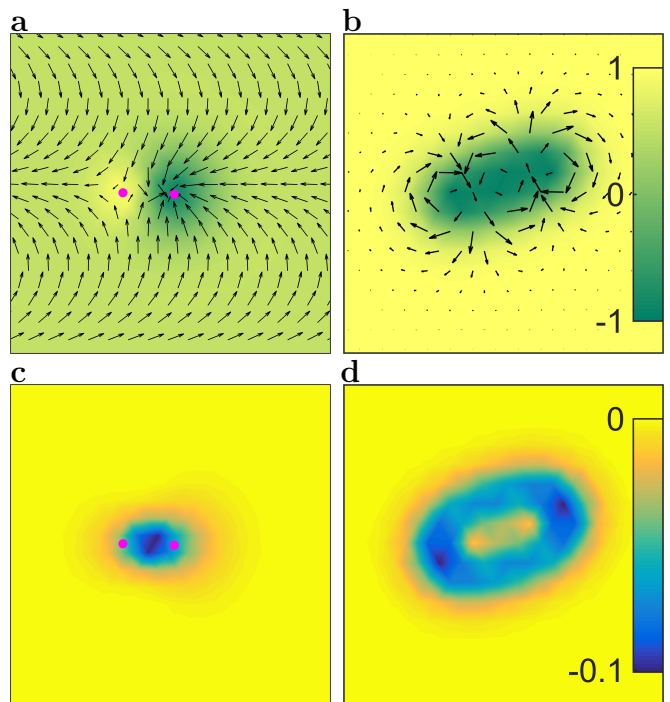


FIG. 4: (a) Bi-meron in the CS state, (b) skyrmion with topological charge 3 in the FM state, and the corresponding distributions of the topological charge density (panels c and d). In-plane spin components are shown with arrows; the out-of-plane spin components and the topological charge density are color coded. Pink dot marks the (anti)vortex center.

corresponding to rotation of the in-plane spins, and the rotational center-of-mass motion [39, 40] (see Fig. 5a and Supplementary Movie 1). Surprisingly, the bi-meron motion in the CS state only depends on the direction of \mathbf{j}_c in the initial stage. In the steady state, the bi-meron moves along a straight line perpendicular to the spiral wave vector \mathbf{Q} and its helicity remains constant (see Fig. 5b and Supplementary Movies 2–3). The spin-Hall torque results in a sinusoidal modulation of S^z in layer 1 and the interlayer interaction attracts bi-merons into a ‘channel’ perpendicular to \mathbf{Q} , located under the $S^z \approx +1$ line in layer 1. The channel position and the skyrmion helicity do depend on \mathbf{j}_c , but the direction of motion does not. This peculiar dynamics is a consequence of the rotational invariance of Heisenberg exchange interactions and the fact that the rotation of in-plane spins is equivalent to a translation of the CS along \mathbf{Q} . The transverse motion of bi-merons is accompanied by a slow drift along \mathbf{Q} , which is a finite-size artifact that becomes smaller as the system size increases (see Supplementary information).

Conclusions: In conclusion, centrosymmetric NiBr₂ has a number of properties required to host skyrmion lattices: frustrated exchange interactions, three-fold symmetry axis and magnetic anisotropy tunable by Fe-doping. However, because of the long magnetic modu-

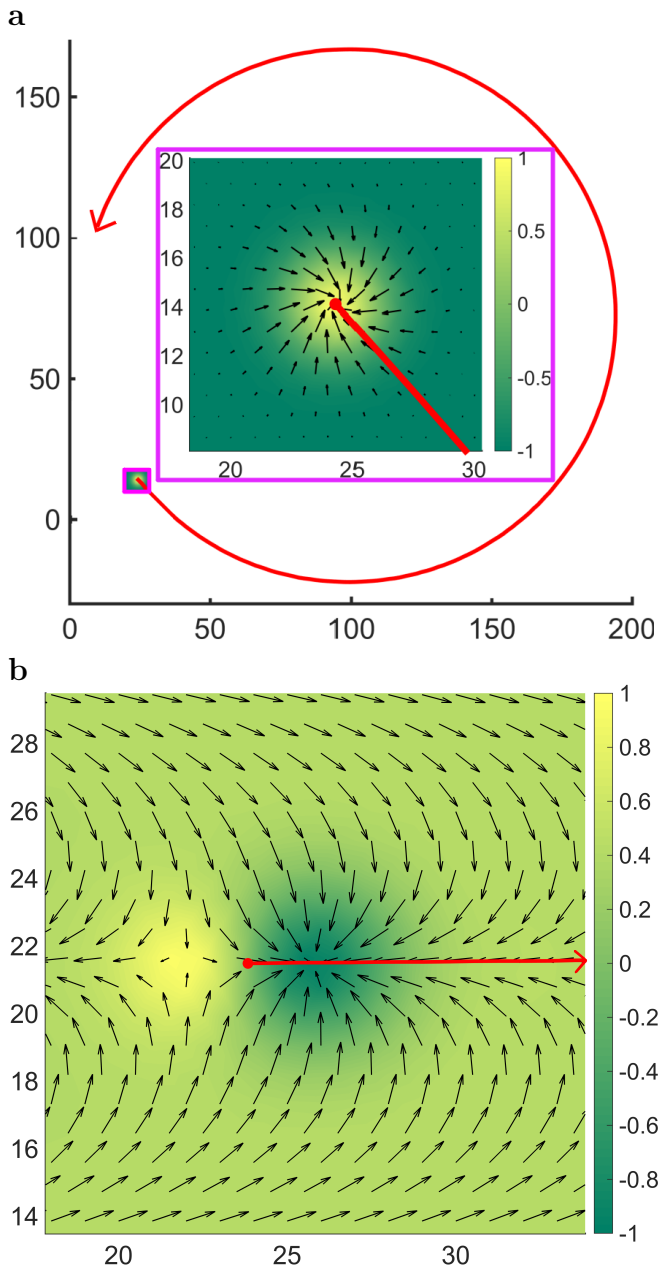


FIG. 5: Trajectories of topological defects in (a) the A-type AFM and (b) CS states moved by the spin-Hall current applied along the positive x direction.

lation period, even the relatively weak AFM interlayer interactions suppress the skyrmion crystal and other multiply-periodic states in this material. Yet the interlayer interactions do not prevent the formation of isolated single-layer skyrmions and even have a stabilizing effect on them. The single-layer skyrmions are mobile, stable in several magnetic phases and, in contrast to AFM skyrmion tubes, can be easily nucleated, which makes them promising candidates for information carriers in antiferromagnetic spintronics.

* Corresponding author; Electronic address: a.pozzi@rug.nl

- [1] S. Mühlbauer *et al.*, *Science* **323**, 915 (2009).
- [2] X.Z. Yu *et al.*, *Nature* **465**, 901 (2010).
- [3] A. Fert, V. Cros, and J. Sampaio, *Nat. Nanotech.* **8**, 152 (2013).
- [4] N. Nagaosa and Y. Tokura, *Nat. Nanotech.* **8**, 899 (2013).
- [5] A. Fert, N. Reyren, and V. Cros, *Nat. Rev. Materials* **2**, 17031 (2017).
- [6] C. Back *et al.*, *J. Phys. D: Appl. Phys.* **53**, 363001 (2020).
- [7] W. Jiang *et al.*, *Science* **349**, 283–286 (2015).
- [8] S. Woo *et al.*, *Nat. Mater.* **15**, 501–506 (2016).
- [9] A.N. Bogdanov and D.A. Yablonskii, *Sov. Phys. JETP* **68**, 101 (1989).
- [10] T. Okubo, S. Chung, and H. Kawamura, *Phys. Rev. Lett.* **108**, 017206 (2012).
- [11] A.O. Leonov and M. Mostovoy, *Nat. Commun.* **6**, 8275 (2015).
- [12] S. Hayami, S.-Z. Lin, Y. Kamiya, and C.D. Batista, *Phys. Rev. B* **94**, 174420 (2016).
- [13] M. Azhar and M. Mostovoy, *Phys. Rev. Lett.* **118**, 027203 (2017).
- [14] S. Hayami, R. Ozawa and Y. Motome, *Phys. Rev. B* **95**, 224424 (2017).
- [15] R. Ozawa, S. Hayami and Y. Motome, *Phys. Rev. Lett.* **118**, 147205 (2017).
- [16] S. Okumura, S. Hayami, Y. Kato, and Y. Motome, *Phys. Rev. B* **101**, 144416 (2020).
- [17] S. Ishiwata *et al.*, Preprint arXiv:1806.02309 (2018).
- [18] T. Kurumaji *et al.*, *Science* **365**, 914 (2019).
- [19] M. Hirschberger *et al.*, *Nat. Commun.* **10**, 5831 (2019).
- [20] N.D. Khanh *et al.*, *Nat. Nanotech.* **15**, 444 (2020).
- [21] M. Hirschberger *et al.*, *Phys. Rev. Lett.* **125**, 076602 (2020).
- [22] A.O. Leonov and M. Mostovoy, *Nat. Commun.* **8**, 14394 (2017).
- [23] Y.A. Kharkov, O.P. Sushkov and M. Mostovoy, *Phys. Rev. Lett.* **119**, 207201 (2017).
- [24] J. Barker and O.A. Tretiakov, *Phys. Rev. Lett.* **116**, 147203 (2016).
- [25] X. Zhang, Y. Zhou, and M. Ezawa, *Nat. Commun.* **7**, 10293 (2016).
- [26] W. Legrand *et al.*, *Nat. Materials* **19**, 34 (2020).
- [27] M.A. McGuire, *Crystals* **7**, 121 (2017).
- [28] S. Jiang, J. Shan and K.F. Mak, *Nat. Mater.* **17**, 406 (2018).
- [29] P. Day, A. Dinsdale, E.R. Krausz, and D.J. Robbins, *J. Phys. C: Solid State Phys.* **9**, 2481 (1976).
- [30] A. Adam *et al.*, *Solid State Commun.* **35**, 1 (1980).
- [31] Y. Tokunaga *et al.* *Phys. Rev. B* **84**, 060406 (2011).
- [32] M.W. Moore and P. Day, *J. Solid State Chem.* **59**, 23 (1985).
- [33] L.P. Régnault, J. Rossat-Mignod, A. Adam, D. Billerey, and C. Terrier, *Journal de Physique* **43**, 1283 (1982).
- [34] P. Day *et al.*, *Solid State Commun.* **51**, 627 (1984).
- [35] S.Z. Lin and C.D. Batista, *Phys. Rev. Lett.* **120**, 077202 (2018).
- [36] K. Katsumata, K. Sugiyama, and M. Date, *J. Phys. Soc. Jpn.* **52**, 3312 (1983).
- [37] J.C. Slonczewski, *J. Magn. Magn. Mater.* **159**, L1 (1996).
- [38] A.V. Khvalkovskiy *et al.*, *Phys. Rev. B* **87**, 020402

- (2013).
- [39] S.Z. Lin and S. Hayami, Phys. Rev. B **93**, 064430 (2016).
- [40] X. Zhang, J. Xia, Y. Zhou, X. Liu, H. Zhang, and M. Ezawa, Nat. Commun. **8**, 1717 (2017).